



Contents lists available at ScienceDirect

## Quaternary International

journal homepage: [www.elsevier.com/locate/quaint](http://www.elsevier.com/locate/quaint)

## The role of mass movements on landscape evolution in the Central Karakoram: Discussion and speculation

John F. Shroder Jr.<sup>a</sup>, Lewis A. Owen<sup>b,\*</sup>, Yeong Bae Seong<sup>c</sup>, Michael P. Bishop<sup>a</sup>, Andrew Bush<sup>d</sup>, Marc W. Caffee<sup>e</sup>, Luke Copland<sup>f</sup>, Robert C. Finkel<sup>g,h</sup>, Ulrich Kamp<sup>i</sup>

<sup>a</sup> Department of Geography and Geology, University of Nebraska at Omaha, Omaha, NE 68182, USA

<sup>b</sup> Department of Geology, University of Cincinnati, Geology/Physics Building, Cincinnati, OH 45221, USA

<sup>c</sup> Department of Geography Education, Korea University, Anam-Dong, Seongbuk-Gu, Seoul, 136-701, Republic of Korea

<sup>d</sup> Department of Earth and Atmospheric Sciences, University of Alberta, Edmonton, Alberta T6G 2E3, Canada

<sup>e</sup> Department of Physics/PRIME Laboratory, Purdue University, West Lafayette, IN 47906, USA

<sup>f</sup> Department of Geography, University of Ottawa, Ottawa, Ontario K1N 6N5, Canada

<sup>g</sup> Department of Earth and Planetary Sciences, University of California, Berkeley, CA 95064, USA

<sup>h</sup> Centre Européen de Recherche et d'Enseignement des Géosciences de l'Environnement, 13545 Aix en Provence Cedex 4, France

<sup>i</sup> Department of Geography, The University of Montana, Missoula, MT 59812, USA

## ARTICLE INFO

## Article history:

Available online xxx

## ABSTRACT

Mass movement constitutes an important process in the evolution of landscapes in mountain regions. However, the role of massive slope failures in denudational unloading and landscape evolution has not been extensively studied. Large-scale mass movements in one of the greatest mountain ranges on Earth, the Central Karakoram in Pakistan, were therefore examined to help evaluate their role in landscape evolution in high mountains. Specifically, four major mass-movement complexes (Ghoro Choh rock avalanche, Busper sackung and slope failure, Gomboro slope failure, and Urdokas rockslide), each comprising  $10^6$  m<sup>3</sup> of debris, were assessed and mapped in detail. Two of these mass-movement complexes, the Ghoro Choh rock avalanche and Gomboro slope failure, were dated using terrestrial cosmogenic nuclides. The ages of occurrence of the mass-movement complexes studied in the Central Karakoram date from the late Pleistocene to the Holocene. The four major mass-movement complexes all involved the removal of mass from the tops of mountain ridges and peaks that failed and were subsequently transported towards the bottom of their respective valleys. Such massive movement of mass is anomalous compared to other forms of mass movement and is generally spatially coincident with exposed deeply buried gneiss-dome structures. These large-scale movements appear to be part of a coupled system involving river incision and glacial debuttrussing, although earthquakes might have triggered these mass movements. This study illustrates the role of climate forcing, which is part of a coupled system of denudational unloading, but it is unclear whether high-magnitude, low-frequency events such as these initiate the isostatic and tectonic influx of mass, or if sustained high-magnitude denudation resulting from a coupled system is responsible for the exhumation of buried structures.

© 2010 Elsevier Ltd and INQUA. All rights reserved.

## 1. Introduction

Recent studies in active young orogens, including the Himalayan-Tibet orogen, show strong interrelationships between tectonics, climate, and surface processes (Hodges, 2000, 2006; Beaumont et al., 2001; Hodges et al., 2001, 2004; Zeitler et al., 2001a,b; Wobus et al., 2003). Numerous studies suggest that high-magnitude erosion and focused denudation of crustal rocks

accelerates uplift and generates extreme relief and anomalously high topography that is governed by erosional–rheological coupling (Koons et al., 2002; Finnegan et al., 2008).

There is considerable debate regarding the role of surface processes in relief production and the magnitude of denudation, although lately, the emphasis has been on fluvial versus glacial erosion in mountain landscape evolution (e.g., Koppes and Montgomery, 2009). Many studies have not adequately taken glacial erosion into consideration, focusing on bedrock river incision and landsliding. In particular, emphasis has focused on threshold slopes, where continuous slope failure is associated with rapid uplift (e.g., Burbank et al., 1996). This coupled system

\* Corresponding author. Tel.: +1 513 5564103; fax: +1 513 5566931.

E-mail address: [Lewis.Owen@uc.edu](mailto:Lewis.Owen@uc.edu) (L.A. Owen).

represents a conceptual landscape evolution model, although it may not produce extreme relief and high surface altitudes given rapid uplift.

Other coupled mass movement systems have not been adequately described throughout the Himalayan-Tibetan orogen. Better understanding of the role of massive slope failures in denudational unloading and uplift is needed. Given the extreme topography and rapid exhumation focused around K2 Mountain in the Central Karakoram of Pakistan as well as the significant aerial extent of massive slope failures in the region, it is an ideal site for evaluating the potential role of glacier coupled mass movement systems. Therefore, the focus was on examining the major landslide complexes in the Central Karakoram, to ascertain the importance of mass movement as a denudational agent and speculate on the role of massive failures in the landscape evolution of this region and other high mountain regions.

## 2. Study area

The Karakoram and its neighboring mountains (Fig. 1) are the result of the collision of the Indian and Asian continental lithospheric plates, resulting in a crustal thickness of >65 km (Molnar, 1988; Searle et al., 1989; Searle, 1991; Foster et al., 1994). A significant component of this collision may be accommodated by extrusion of the Asian plate along continental-scale strike-slip faults striking roughly orthogonal to the direction of convergence (Molnar and Tapponnier, 1975; Tapponnier and Molnar, 1979). One of these major strike-slip faults, the Karakoram Fault, bounds the north side of the Central Karakoram (north of K2). This fault may contribute as much as 10 mm  $y^{-1}$  of lateral offset in accommodating the crustal shortening relating to the Indian–Asian collision (Chevalier et al., 2005; Robinson, 2009). The role of the Karakoram Fault in uplift is unknown, but it is unlikely to be significant enough to explain the great elevation of K2 and its surrounding high peaks. In the southern part of the Karakoram, from the Skardu Basin to K2, a series of Neogene age (6–17 Ma) gneiss domes have been exhumed between the oblique crustal boundaries constituted by the Main Karakoram Thrust (MKT) and the Karakoram Fault. The study area is bounded to the south and north by the MKT and the

Karakoram Fault, respectively, and comprises rocks of the Karakoram metamorphic series, Karakoram granitoids, Gasherbrum sedimentary deposits, Gasherbrum diorite and the K2 and Muztagh Tower gneisses (Searle et al., 1989; Searle, 1991).

The Karakoram alone contains four of the world's 14 peaks higher than 8000 m above sea level (asl) and >60 peaks higher than 7000 m asl. The Central Karakoram contains deep glaciated valleys with kilometers of vertical relief. Large landslides are abundant throughout the region and represent significant areal coverage of the landscape. Altitudes below 3000 m asl are submontane with fluvial and aeolian processes dominating the environment (Hewitt, 1989; Seong et al., 2009). Intermediate altitudes (subalpine and high alpine zones) are characterized by active paraglacial processes and postglacial rock debuitressing-induced landslides, and outburst floods (Hewitt, 1989; Seong et al., 2009). Glaciers and snowfields become more dominant with increased altitude, with perennial ice at high altitudes covering many of the very highest slopes, ridges and peaks (Seong et al., 2009). The region has been extensively glaciated with evidence preserved for at least six major glacial advances over the last couple of glacial cycles (Seong et al., 2007).

The climate of the region is transitional between central Asian mid-latitude (dominated by the mid-latitude westerlies) and Indian summer monsoon types, but there is considerable microclimatic variability influenced by multi-scale topographic factors (Hewitt, 1989; Seong et al., 2007, 2009). At Skardu (~2180 m asl), the average annual temperature is ~12 °C and the mean annual precipitation is ~200 mm (Seong et al., 2007). The highest precipitation occurs during spring as the mid-latitude westerlies advance into the region. Two-thirds of snow accumulation in the Central Karakoram occurs in winter and spring, supplied by mid-latitude westerlies, while the other third is supplied from the Indian monsoon during summer (Hewitt, 1989; Seong et al., 2007, 2009).

## 3. Methodology

Standard geomorphic mapping, rock sampling, and ground photography constitute a major portion of this work. Satellite

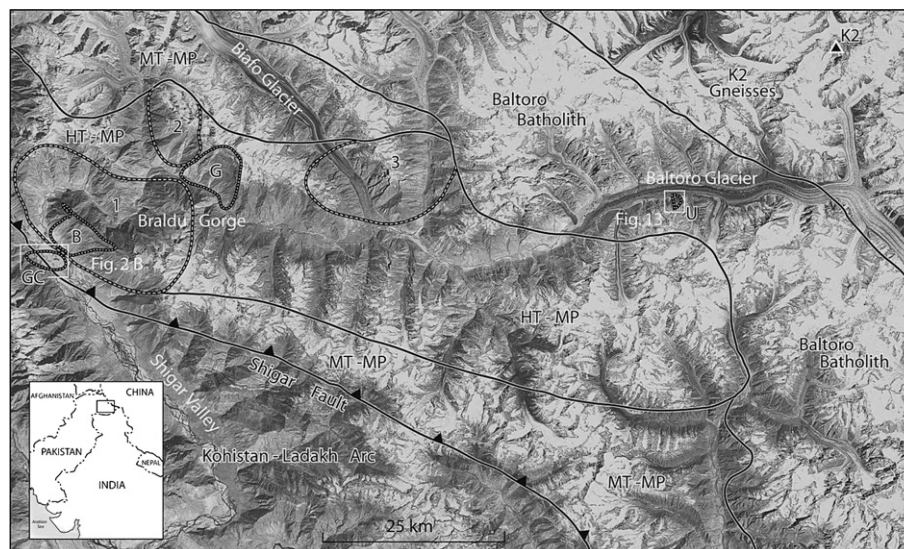


**Fig. 1.** Location of study area in the Karakoram and index map of Shigar–Braldu–Baltoro area of northeast Pakistan, based on a Landsat satellite image mosaic. Migmatic foliation domes (1 – Dassu; 2 – Ho Lungma; 3 – Askole–Panmah); HT-MP (high temperature – moderate pressure metamorphic rocks); MT-MP (moderate temperature and pressure metamorphic rocks) (after Searle, 1991; Mahéo et al., 2004; geologic boundaries are approximate at this large-scale). GC – Ghoru Cho rock avalanche complex; B – Busper sacking and slope-failure complex; G – Gomboro slope-failure complex; U – Urdokas rockslide and slope-failure complex.

imagery from four decades of image acquisition (Corona, Keyhole, Landsat MSS, ETM, SPOT, ASTER) was used to identify large mass movements on the landscape and assisted in field investigation during summer 2005. Landslides were mapped throughout the Shigar and Braldu valleys, and along Baltoro Glacier. Four major mass-movement complexes were mapped and studied in detail: the Ghorohoh rock avalanche; the Busper sackung and slope failure; the Gomboro slope failure; and the Urdokas rockslide (Fig. 1).

Samples for terrestrial cosmogenic nuclide (TCN) surface exposure dating were collected from the surfaces of boulders on high positions where no evidence of exhumation or slope instability was apparent on two landslide deposits (the Ghorohoh rock avalanche and Urdokas rockslide). Four to seven boulders from each landslide were sampled and dated to provide a check on the reproducibility of the ages and on the possibility of the inheritance of TCNs by prior exposure to cosmic rays. Each boulder was photographed, measured, and the degree of weathering and site conditions were recorded. The hemispherical angle of inclination from the boulder site to the tops of the surrounding mountain ridges and peaks was measured to estimate the topographic shielding coefficient.

Boulders that contain quartz were prepared for  $^{10}\text{Be}$  TCN analysis. This was undertaken in the geochronology laboratories at the University of Cincinnati. First, the samples were crushed and sieved. Quartz was then separated from the 250 to 500  $\mu\text{m}$  size fraction using the methods of Kohl and Nishiizumi (1992). After addition of Be and Al carriers, Be and Al were separated and purified by ion exchange chromatography and precipitation at  $\text{pH} > 7$ . The hydroxides were oxidized by ignition in quartz crucibles. BeO was mixed with Nb metal and loaded onto targets for determination of the  $^{10}\text{Be}/^9\text{Be}$  ratio by accelerator mass spectrometry at the Center for Accelerator Mass Spectrometry in the Lawrence Livermore National Laboratory. Isotope ratios were compared to ICN  $^{10}\text{Be}$  and NIST  $^{26}\text{Al}$  standards prepared by Nishiizumi et al. (2007) using a  $^{10}\text{Be}$  half-life of  $1.36 \times 10^6$  yr. TCN  $^{10}\text{Be}$  concentrations were then converted to zero-erosion exposure ages using sea-level high-latitude (SLHL)  $^{10}\text{Be}$  production rate of  $4.5 \pm 0.3$  atoms  $\text{g}^{-1}$  of  $\text{SiO}_2$   $\text{a}^{-1}$  (Stone, 2000; Balco et al., 2008).  $^{10}\text{Be}$  production rates were scaled to the latitude and elevation of the sampling sites using the scaling factors of Stone (2000) with 3% SLHL muon contribution. There is still debate concerning the correct scaling method and SLHL rate, possibly impacting the model exposure age by  $\sim 15\%$  (Owen et al., 2008), and therefore, quoted ages have not been corrected for variations in the geomagnetic field. Owen et al. (2008) discuss these concerns for Himalayan and Tibetan study regions.

Boulders on the Ghorohoh rock–avalanche complex (lobes I & II in Hewitt, 1999, that is, the central and eastern lobes) that did not contain quartz were analyzed for whole-rock  $^{36}\text{Cl}$  TCN methods. Samples were taken from relatively flat lying surfaces so that no geometric corrections were needed and to avoid possible periglacial debris cover. All the samples taken were prepared at the Purdue Rare Isotope Measure (PRIME) Laboratory for whole-rock  $^{36}\text{Cl}$  analysis outlined by Stone et al. (1996). Samples were crushed and the 250–500  $\mu\text{m}$  fraction was collected. To remove carbonate and potential meteoric  $^{36}\text{Cl}$  contaminations, crushed samples were leached thoroughly, first in 18 M  $\Omega$  water, and then in 10%  $\text{HNO}_3$  for more than 12 h at room temperature. Major elements, including U and Th, were determined by X-ray fluorescence before and after leaching, and B and Gd were detected by prompt-gamma-emission spectrometry. The aliquots for elemental analysis were collected before and after leaching. The samples were dissolved over 2 days in a 15 M HF/2 M  $\text{HNO}_3$  mixture at 60–70  $^\circ\text{C}$ . Approximately 1 mg of chloride carrier was added to increase the final sample size and decrease the propagation of chloride concentration measurement

errors in the calculation of  $^{36}\text{Cl}$  concentrations. Chloride was recovered from the sample solutions as AgCl and then redissolved in dilute  $\text{NH}_4\text{OH}$ . Sulfate was coprecipitated with AgCl and then removed by precipitation of  $\text{BaSO}_4$ . Removal of sulfur is essential due to interference of isobaric  $^{36}\text{S}$  with  $^{36}\text{Cl}$  in the AMS measurements. Pure AgCl for AMS was re-precipitated by acidification, recovered, washed, dried, and packed into accelerator targets.

The samples were measured at the AMS facility in PRIME Lab. The numbers of cosmogenic  $^{36}\text{Cl}$  atoms were converted into ages using the web-CN programmed by the PRIME Laboratory. Elevation–latitude scaling was based on Lal (1991) and Stone et al. (1996), and muon production was referenced from Phillips et al. (2001). Spallation production constants for  $^{36}\text{Cl}$  from Ca and K (66.8 and 154 atoms  $\text{g}^{-1}$   $\text{yr}^{-1}$ ) derived by Phillips (1995) and Phillips et al. (1996, 2001) were applied for age calculation. All ages were produced using a bulk density of  $2.8 \text{ g cm}^{-3}$  and a neutron attenuation coefficient of  $170 \text{ g cm}^{-2}$ . The analytical error for  $^{36}\text{Cl}$  ages is assumed to be  $\leq 8\%$  of the age (Phillips, 1995; Phillips et al., 1996).

#### 4. Ghorohoh rock–avalanche complex

An impressive series of large hummocks rising up to 50 m above the valley floor and containing boulders up to 10 m in diameter are present along the upper Shigar Valley near the confluence of the Braldu and Shigar rivers (Fig. 2). Oestrich (1906) first identified these landforms and believed they formed by rock avalanching. Dainelli (1922) later reinterpreted them as moraines. However, Hewitt (1998, 1999) reconfirmed this as a catastrophic rock avalanche that had advanced into the Shigar Valley from the southwest valley wall in the early to middle Holocene. The proximity of the Ghorohoh to the Busper sackung and slope-failure complex (see next section) on the opposite northeast valley side suggest a possible genetic interrelationship between the two failures.

The Ghorohoh rock avalanche developed largely from tonalitic crystalline rocks of the Kohistan–Ladakh Arc complex. This avalanche is adjacent to the intersection of the Shigar Fault strand of the MKT suture and the Karakoram metamorphic complex of metasediments and gneisses in which the Busper sackung has developed on the other side of the Shigar Valley (Mahéo et al., 2004). The presence of two major slope-failure complexes in such proximity to each other as well as to where the MKT crosses the upper Shigar Valley from one side to the other, further suggests possible genetic interrelationships.

According to Hewitt (1999), the Ghorohoh rock avalanche complex represents three main events that dammed the Basha and Shigar rivers, apparently at different times, displacing considerable amounts of fluvial and lacustrine sediment that had been deposited in the Shigar Valley. This study was not able to confirm or deny the evidence of three different failure times and therefore cannot test Hewitt's (1999) interpretation. The rock avalanche comprises  $\gg 10^6 \text{ m}^3$  of debris, and its main source scarp is a smooth planar rock facet high on the southwest valley wall (Fig. 2). This feature extends up to 1 km in length and comprises profuse broken boulders. As with similar features in other mountain environments, there are abundant syn-failure scars and clast lineations (Shroder, 1998; Hewitt, 2002).

Using geomorphic mapping and  $^{10}\text{Be}$  TCN dating, Seong et al. (2007) demonstrated that a long glacier retreated from the Shigar Valley during the Late Glacial. Hewitt (1999) obtained a radiocarbon date of  $\sim 7.1$  ka on deformed lake deposits that were affected by the avalanche, thus supporting a Holocene age for the landslide. The Ghorohoh I lobe overtopping the lake sediments has several sub-lobes (Fig. 2). The large spread of  $^{36}\text{Cl}$  ages (4–40 ka; Table 1) suggests that surfaces and boulders have been

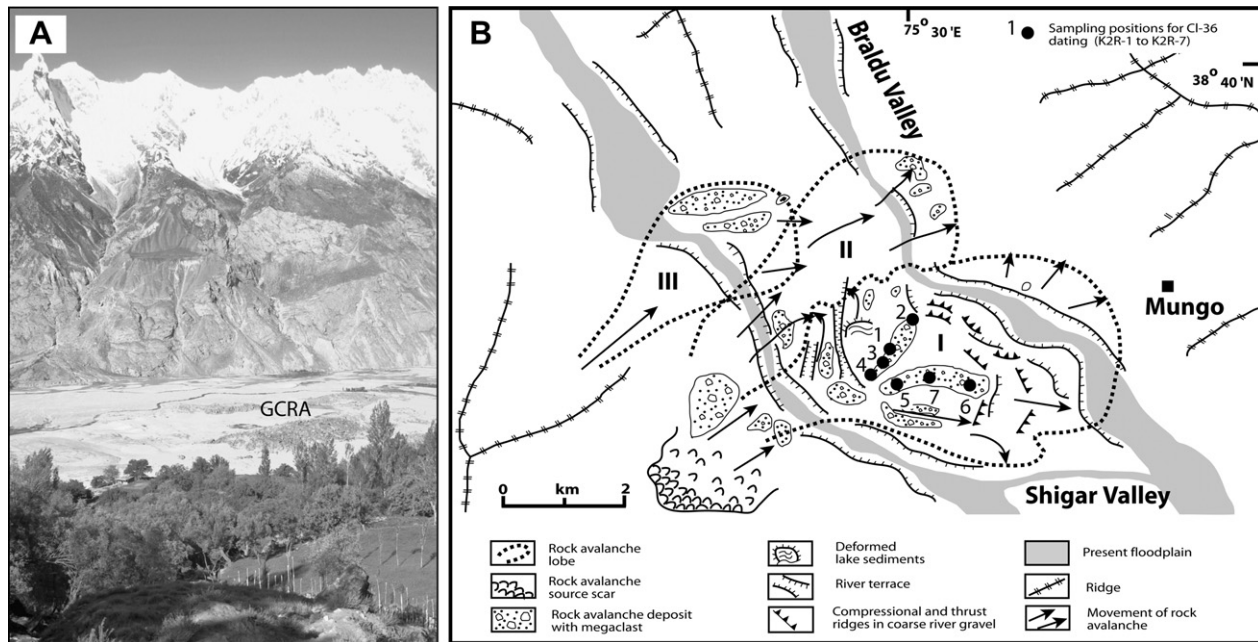


**Fig. 2.** The Busper slope failure and the Ghorcho rock avalanche (GCRA). (A) View southwest from the middle of the irrigated Busper slope-failure complex down into the Shigar Valley and the piles of rock debris from the Ghorcho rock avalanche complex in the valley bottom, as well as the planar slip surface on the opposite valley wall (light-colored smooth triangular shape about half way up on the center-right) below the snow, glaciers, and darker tundra vegetation. Mahéo et al. (2004) mapped the trace of the Shigar Fault (or MKT) at the base of this valley wall, whereas Searle (1991) mapped it through the middle of the Busper slope failure, approximately from where this picture was taken. (B) Geomorphic map of the Ghorcho rock avalanche (adapted from Hewitt, 1999) showing sampling positions for the TCN dating.

significantly weathered and/or toppled, and the oldest  $^{36}\text{Cl}$  ages (K2R-1 and -2) are probably due to inherited TCNs where the boulders had prior exposure to cosmic rays. Sub-lobes A and B have minimum  $^{36}\text{Cl}$  ages of  $\sim 4.0$  and  $\sim 5.3$  ka, respectively. Disregarding the two oldest TCN dates, the exposure ages indicate that the Ghorcho rock-avalanche complex must be Late Glacial or Holocene. These ages are consistent with the morpho-stratigraphy, which indicate that the avalanche occurred after the retreat of the glacier.

The fundamental causes of the Ghorcho rock avalanches are not known with certainty; seismicity in this heavily faulted structural environment is always a possibility. The narrow spur extension of the Haramosh Range here, between the Basha-Shigar rivers on the northeast and the nearly parallel Indus River on the southwest, is cut through by a series of northeast-flowing, small glaciers that have severely dissected the landscape to leave a number of precipitous and isolated glacial horns, one or more of which were probably sources for the slope failure.

## 5. Busper sacking and slope-failure complex

First discovered on stereographic Corona satellite imagery from the 1960s, the snowline delineation of a huge and sharp ridge-top graben shape suggest massive slope failure of the slopes on both

sides of the Bhaldu–Shigar confluence, and deep into the ridge (Figs. 1 and 3). With  $\sim 2200$  m of overall relief, the ridge-top graben clearly extends  $\sim 5$  km lengthwise along the ridge, and probably as much as 9 km to the northwest. Field assessment shows that it has propagated downslope failure on the southwest-facing slope below the uppermost ridge-top graben for another 4–5 km. The failure surfaces within the mountain slope have developed in antiformal oriented Dasso gneisses and Ganschen metasediments in the hanging wall of the MKT. The Busper sacking is developed in migmatitic gneisses on top of the Dasso gneiss dome, which has formed as a result of diapiric ascent of partially molten mid-crustal rock in a compressive regime aligned along the dextral, strike-slip Shigar Fault part of the MKT (Mahéo et al., 2004). Exhumation of these rocks in the Pleistocene was  $\sim 5$  km (Foster et al., 1994). The exposed 3000-m high part of the Busper sacking itself therefore constitutes only a surficial part of the present-day manifestation of that exhumation.

The orientations of foliation and lineations in the Dasso gneisses are antiformal, with the result that they roughly parallel to the slopes on both sides of the Busper ridge. In addition, sheeting joints also were also observed to parallel the southwest slope of the ridge, which together with the conformal foliation and lineation within the slope, contribute to failure potential. The gneisses of the Busper

**Table 1**

Sampling locations and  $^{36}\text{Cl}$  ages and major elemental compositions of boulders on the Ghorcho rock avalanche in Shigar Valley near the village of Mungo.

Sample ID	Latitude ( $\pm 0.001^\circ\text{N}$ )	Longitude ( $\pm 0.001^\circ\text{E}$ )	Altitude (m asl)	K <sub>2</sub> O (%)	CaO (%)	Cl (ppm)	$^{36}\text{Cl}/^{35}\text{Cl}$ ( $10^{-15}$ )	$^{36}\text{Cl}$ exposure age (ka)	Sample location on rock avalanche
K2R-1	35.644	75.498	2371	1.16	5.0	30.772	1345 $\pm$ 75	40.3 $\pm$ 2.3	Ghorcho Choh I (sublobe A)
K2R-2	35.644	75.498	2389	0.28	10.6	34.253	1238 $\pm$ 127	35.0 $\pm$ 3.7	
K2R-3	35.638	75.498	2399	0.27	10.7	109.731	202 $\pm$ 16	5.3 $\pm$ 0.4	Ghorcho Choh I (sublobe B)
K2R-4	35.644	75.497	2393	0.35	10.6	51.390	404 $\pm$ 36	10.9 $\pm$ 1.0	
K2R-5	35.639	75.502	2392	0.19	10.8	16.575	159 $\pm$ 23	4.0 $\pm$ 0.6	
K2R-6	35.640	75.518	2396	0.20	10.2	26.373	587 $\pm$ 44	16.2 $\pm$ 1.2	
K2R-7	35.642	75.519	2397	0.22	10.6	34.479	352 $\pm$ 26	9.2 $\pm$ 0.7	

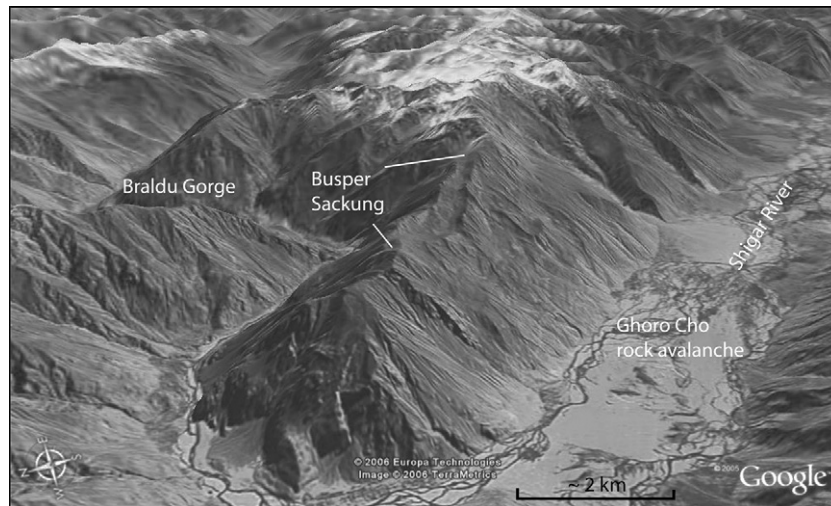


**Fig. 3.** View southeast along the Busper ridge-top graben sacking showing the slope-failure complex on the southwest-facing (right) side. The Braldu River Valley occurs on the left and the broad Shigar Valley on the right. Several dark-colored patches of rock fragments from the Ghoro Cho rock avalanche complex may be discerned in the middle of the Braldu–Shigar braid plain on the lower right. The pronounced concavity of the Gomboro rockslide complex can also be seen in the upper left along the right (north) bank of the Braldu River (from Google Earth™ satellite imagery draped over a digital elevation model).

sacking are also highly micaceous, and in a few places are partly schistose, which were weathered in many locations. The amount of rock and debris that moved or is moving due to the sacking is difficult to estimate because the depth of the failure is not known; however it is likely to be  $\gg 10^7 \text{ m}^3$ .

The Busper sacking formed inside a tight bend in the confluence of the Braldu–Shigar rivers. The northeast side of the ridge is much steeper ( $52^\circ$ – $60^\circ$ ) and narrower at 2–2.5 km wide, whereas the southwest slope is more gentle ( $25^\circ$ – $35^\circ$ ) and wider (4–5 km). This topographic asymmetry suggests that the sacking failure involves the steeper northeast side, but field observations show that the only active and past motion has occurred on the gentler southwest side; with vertical subsidence of the ridge-top graben on the order of several hundred meters. The internal space-accommodation problem produced by long-term subsidence of the graben has been accomplished by numerous upward and outward

shears in the crystalline gneisses. This has resulted in profuse open fractures, and antislope scarps and subsidiary rotational slumps in the slope colluvium and sheared bedrock (Fig. 4). The sheeting joints that have developed in the crystalline rock parallel to the hillslope also helped contribute to the development of colluvial boulders, as well as to the overall mass movement.

The uppermost Busper graben is a prominent subsidence trench with high, knife-edged ridges and basal rock-fragment subsidence structures where the ground surface seems to be dropping and folding inward or invaginating and thus collapsing internally on itself (Fig. 5). Paludal, lacustrine and fluvial sedimentation in the graben has produced a 3–4 m thick (and perhaps much more) deposit. A subsequent breach in the graben wall, perhaps caused by further sacking development, has allowed trapped water to escape, and has trenched the graben-fill sediments to provide good exposures. These were sampled for luminescence dating and they

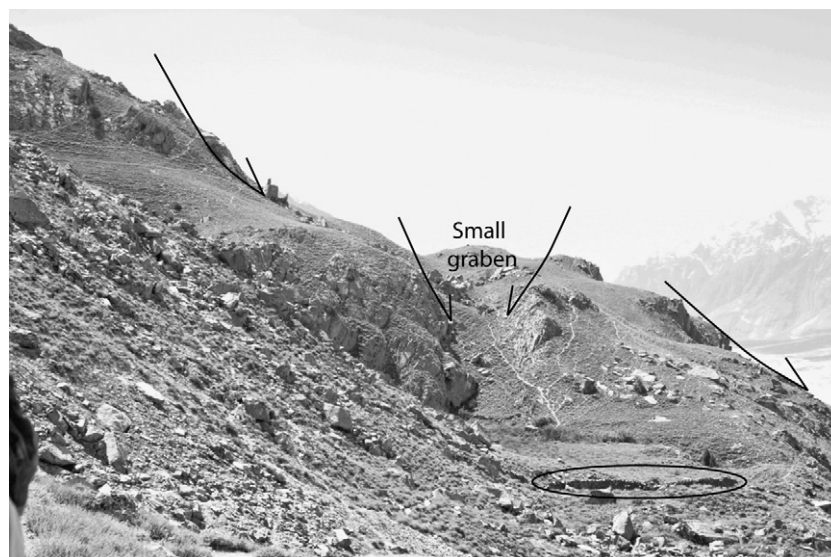


**Fig. 4.** Antislope scarps and slumped zones of rock and debris that formed in about the middle of the southwest-facing slope of the Busper slope-failure complex. The arrows show displacement surfaces. The stone wall (encircled by the ellipse) in the lower right hand portion of the photograph provides a scale.

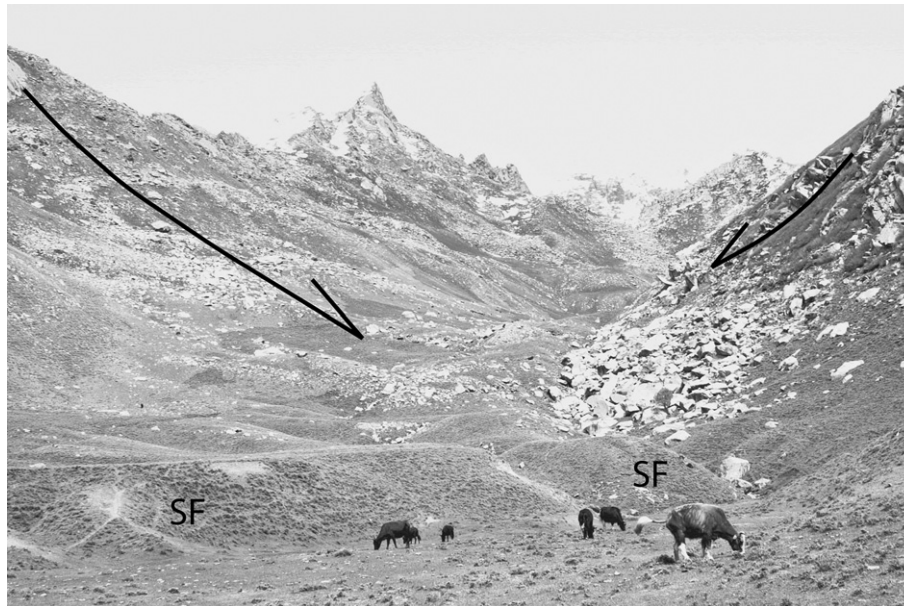


**Fig. 5.** The interior of the uppermost graben of the Busper sackung looking southeast. The terraced infilling (foreground above cows) represents at least 3–4 of clastic infilling that is now breached and eroded (labeled SF). Note the boulders at center right that seem to be invaginating or folding down and inward into the slope. The steep hillslope block to the far right is moving to the right and downward. The steep hillslope to the left (northeast) is one of the main sackung slip planes exposed at the surface, highlighted by the large arrow that indicates the displacement direction.

yielded a Late Holocene OSL age. The sediments, however, had high dose rates ( $\sim 10$  Gy/ka) due to high U concentrations and therefore OSL ages cannot be quoted with any confidence, except to show they are at least Holocene in age.

The melt water originating in the graben passes downslope, and although much goes into the numerous open fissures along the way, enough passes over the rock surfaces, or reemerges as springs, so that the well-watered village of upper Mungo, below the sackung, is quite fertile with numerous large trees, orchards, and wheat and potato crops. The reasonably level site of Mungo, situated on an otherwise fairly steep hillside, is actually the top of a large compound slump block that has formed from fractured bedrock and profuse colluvium. The fresh main scarp and subsidiary scarp subsidence around the top edges of the block are one to several meters high and are light in color. These attest to the ongoing slope activity.

The contemporary activity of the Busper sackung and the natural precipitation catchment it creates at an altitude of  $\sim 4500$  m asl means that this feature has every likelihood to continue developing. Whether or not the sackung will ever exceed some shear-strength threshold and move catastrophically cannot be determined at present. The depth of sediment in the upper graben and the breaching of the outer graben wall together indicate that the feature already has a long history, perhaps spanning much of the Holocene, and so will likely continue with slow movement into the future. The first of the original subsidence adjustments most likely began as a result of deglaciation downwasting and debuttressing in the Late Glacial and early Holocene, and/or as a result of undercutting of the valley wall by the Shigar River that was forced against it in the middle Holocene when the Ghoru Choh rock avalanche displaced the river about 7000 y ago (Hewitt, 1999). Apparently the process has continued over the many millennia until the present. Earthquakes may have triggered some of the individual slope movements in the sackung, but this is not possible to determine.

Other unusual fracture-related phenomena, such as additional sheared ridges and a prominent pinnacle or horst-like block (Fig. 6) to the northwest along the strike of the Busper ridge, provide

evidence that the Busper massif is continuing to collapse in a massive sackung, but the depth to which the sackung fractures penetrate is unknown. Shallow, intermediate, or deep fracture systems may be present as illustrated on the hypothetical cross-sections shown in Fig. 7, and these various interpretations need to be tested in future work. However, the fact that only the more gentle southwest side of the Busper ridge seems to be actively failing is anomalous. The steeper northeast side may also have antislope fractures that have not yet been detected. Only relatively minor rockslides have been recognized on the upper portions of that side to date.

## 6. Gomboro slope-failure complex

This mass-movement complex is located on both sides of the Braldu River gorge just upstream from the settlements of Chapok and Gomboro (Figs. 1 and 8). Hewitt (1998) was the first to describe the Gomboro slope-failure complex and noted that it was a tripartite complex. A new jeep road on the southern bank of the Braldu gorge allowed examination of the cross-river toe of the feature, but it was not possible to access the main body of the landslide on the northern side of the Braldu River. Nevertheless, samples were obtained for  $^{10}\text{Be}$  TCN dating. Details of the complex, polyphase deformational and emplacement history on the southern side of the Braldu gorge were examined. This was briefly introduced in Seong et al. (2007, 2009), who called the Gomboro landslide the Chapok landslide.

The Gomboro slope-failure complex developed in strongly weathered, weak metasediments of the Ganschen unit, which are dominated by pelites (originally shales) with lesser amounts of interbedded marble and amphibolite. The structural location of this slope failure is at the east margin of the Ho Lungma gneiss dome (Fig. 1), which resembles the Dassu dome, but which has not been studied in as much detail (Mahéo et al., 2004). A northeast-dipping overthrust sheet of the Dumordu unit metasediments (predominantly marble, with minor interbedded amphibolites, pelites, orthoquartzites, metaconglomerates, and other similar units) occurs at the top of the  $\sim 6000$  m asl mountain ridge (Tango to



**Fig. 6.** Horst-like pinnacle at northwest end of Busper graben and ridge with associated shear planes that appears to be the result of subsidence and failure of other rock around it.

Gama Sokha Lumbu) at the head of the failure. Field examination of the  $\gg 10^6 \text{ m}^3$  landslide mass revealed many 'rotten' highly weathered boulders of schist in which the micas had preferentially decomposed. In addition, the basal shear plane beneath the slope failure now outcrops along the Braldu River that has downcut several to tens of meters below it, and is marked by extensive mineral-salt-laden seeps and grassy vegetation around which white crystal precipitates exist (Fig. 9).

The Gomboro slope-failure complex measures  $\sim 4 \text{ km}$  wide and  $\sim 3 \text{ km}$  long, with a main scarp of at least a kilometer in long and wide, and a vertical displacement of rock below that of perhaps another  $1.5\text{--}2 \text{ km}$  (Fig. 8). The initial failure crossed the Braldu River and dammed it to a depth of at least  $200 \text{ m}$ . Lacustrine sediments occur  $\sim 6 \text{ km}$  upstream on the right bank of the Braldu River at Chongo, which are probably associated with the Gomboro failure, rather than with the smaller failure into which they are intermixed.

The toe of the Gomboro slope failure extends along the left bank of the Braldu River for about a kilometer, with a brandung (Heim, 1932; Hewitt, 2002) distal ridge  $1\text{--}10 \text{ m}$  high along the distal contact with the south valley wall. New rockfall material comprising granite melt pods from the steep rock walls on the south have traversed the toe in the recent past and are distinctive because they are of different lithology from that of the metasediments of the main slope failure. In fact, the common ongoing occurrence of such rockfalls from the south wall of the gorge is well known, especially because a lead climber of the Chinese K2 team was killed in early summer 2005 when a rockfall from the south-side cliff wall struck his jeep as he was driving across the landslide.

The main body of the landslide complex comprises an open matrix of clast-supported rock rubble into which weathered surficial fine materials have trickled downwards. The surficial fines, probably remnants of the dust and ground-up rock flours of the original emplacement, support growth of a black and gray lichen and moss. This is very similar in appearance to the surface of the 1841 landslide across the Indus at Lichar below Nanga Parbat reported by Shroder (1993). In addition, the Gomboro failure complex is characterized by a profusion of terracettes, multiple small ( $1\text{--}3 \text{ m}$ ) slip plane scars with tread and riser configurations active indicating slope movement (Fig. 10). This is also a characteristic feature of the 1841 landslide at Nanga Parbat, and attests to either the youth of the main failure, or to recurrence of subsidiary activity, which appears to be the most likely case here.

The main mass of the slope failure on the north side of the Braldu River is trenched by at least three major nalas (gulleys), which provide evidence of internal instability and ongoing failure (Fig. 10). The ongoing activity, profuse rubble, and steep slopes of the main slope failure mass have provided a ready source of clastic debris for remobilization in the two big and one small debris-flow nalas that exist here. All the nalas have large multiple inset (as many as 7) or overlapping distal lobes, now truncated by the Braldu River, where slurries of rocks and mud from the rapid, wet debris flows debouched at river level, partially and periodically blocking the Braldu River.

The afore-mentioned toe of the main slope failure downstream along which the new jeep road passes, is matched on the north bank by an area of light, buff-colored talus, and a  $\sim 200\text{-m}$ -high incision cliff cut through the slope-failure diamicton. At the top of this occurs a long, downstream sloping ( $\sim 10^\circ$ ) terrace some  $\sim 10\text{--}20 \text{ m}$  thick, with plane bed stratigraphy attesting to breakout flood waters that washed over it at high velocity. Below this terrace the landslide toe is cut  $\sim 200 \text{ m}$  down to the bedrock beneath. A narrow epigenetic gorge superimposed into the bedrock, first recognized by Hewitt (1998), occurs just upstream from the breakout flood terrace. The entire Braldu River discharge is forced through this narrow ( $< 10 \text{ m}$  wide) bedrock slot. The river here is a roaring, high velocity mass of foaming water and this is the only significant bank-to-bank bedrock exposure along the entire length of the river from the Baltoro Glacier terminus to the Braldu River confluence with the Shigar River. Otherwise the entire river valley from glacial source to its Shigar junction is choked with profuse mass movement and glacial debris that obscures the bedrock.

The  $\sim 200 \text{ m}$  deep breakout flood of the Gomboro, which caused the initial superposition of the Braldu across the bedrock spur, was also responsible for the movement of large boulders downstream. At Chapok near the landslide toe, as well as just below the Dassu Police Post, Seong et al. (2009) measured flood-rounded boulders  $> 10 \text{ m}$  in diameter and dated the breakout flood to be Mid- to Late Holocene in age using  $^{10}\text{Be}$  TCNs. Significantly, however, none of the eight boulders that were sampled dated close to the time of the landslide failure (see below). Rather most seemed younger or far older, which suggests that many other flood events have occurred in the region.

Dating of the Gomboro slope-failure complex is somewhat problematic because the feature appears to have had a complex history of failure as ice retreated up the valley at the end of the last

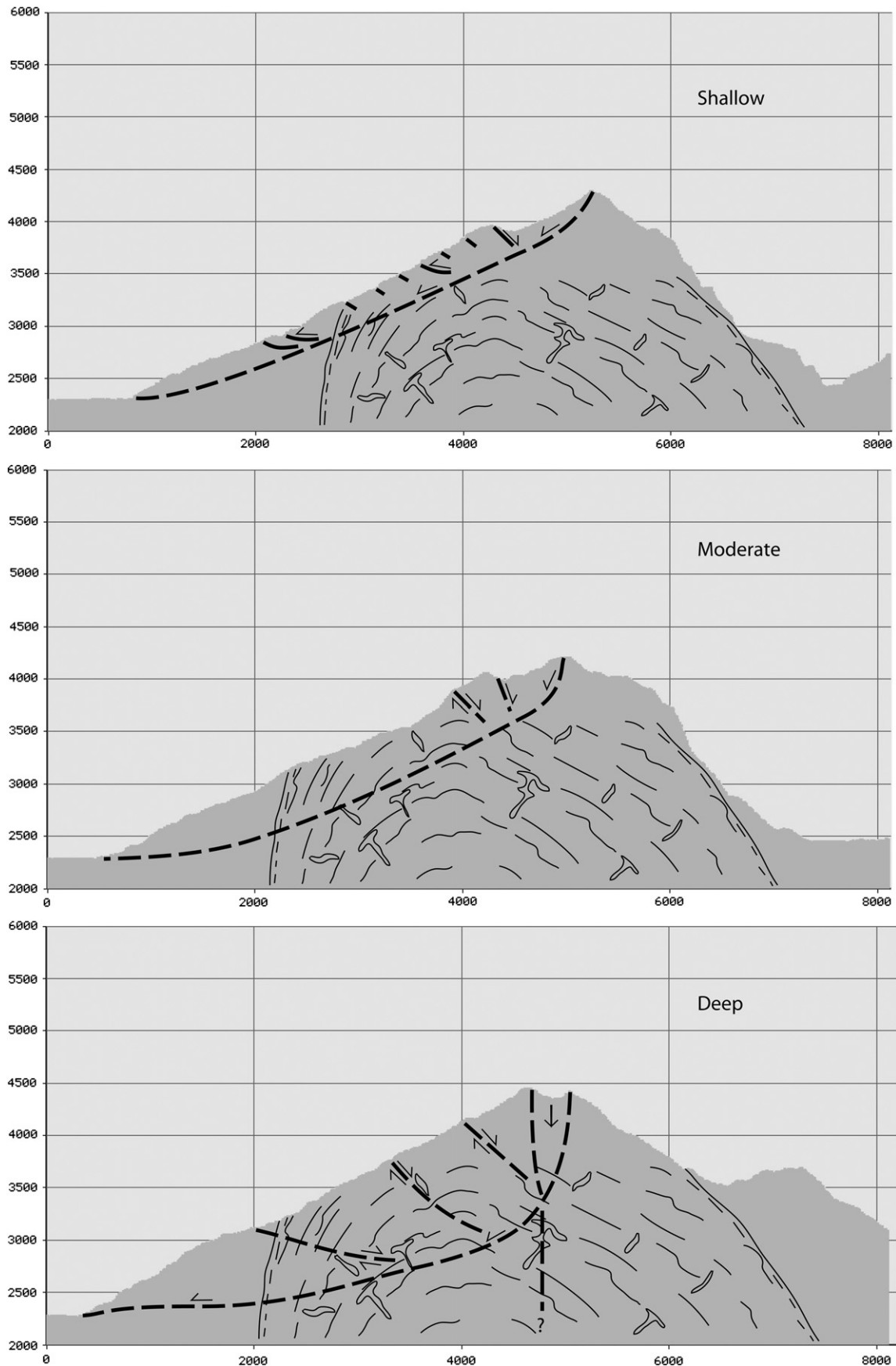
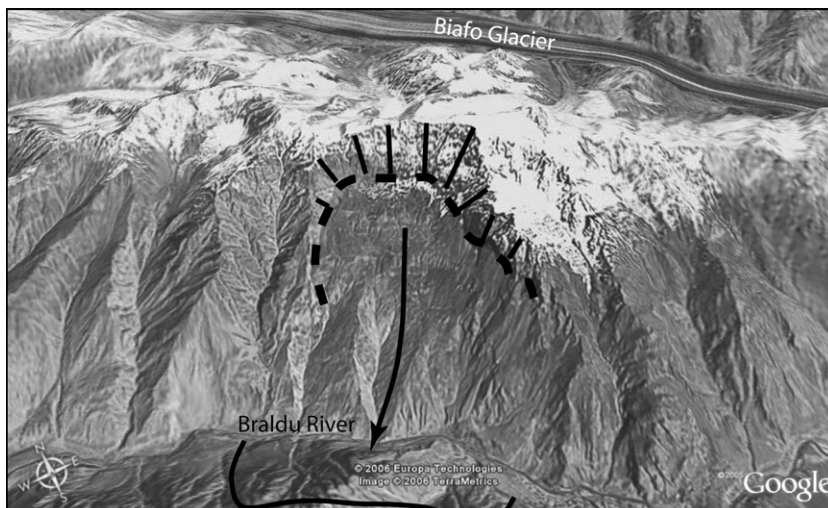


Fig. 7. Multiple cross-sections from northwest to southeast of Busper sackung constructed from an ASTER imagery-based DEM showing schematic of possible internal structure organized into shallow, intermediate, and deep versions of possible internal sackung failure surfaces. Internal foliation of the Dassu Gneiss dome shown is from Mahéo et al. (2004).



**Fig. 8.** Image of the Gomboro rockslide slope-failure complex in the figure center; view looking approximately north from the south side of the Braldu River. Part of Biafo Glacier appears in the background. The Gomboro failure is marked by a predominant concave or scoop-shaped up area below a huge main scarp, highlighted by subvertical lines (images acquired from Google Earth™). The large arrow indicates the run out direction.

glacial (Seong et al., 2007). Six  $^{10}\text{Be}$  exposure ages (Table 2) from boulders in the slope failure range from  $13.1 \pm 0.5$  to  $15.8 \pm 0.5$  ka, whereas two  $^{10}\text{Be}$  exposure ages from glacially eroded surfaces above the landslide on the south valley side date to  $10.8 \pm 0.3$  and  $11.1 \pm 0.3$  ka (samples K2-31 & K2-33 in Seong et al., 2007, recalculated using the scaling model and production rates listed above). The slightly older ages on the rockslide can be explained by inheritance of TCNs if they had been exposed to cosmic rays prior to deposition. This is likely because the samples were collected from an area near the leading edge of the rockslide and were probably carried down while preserving the relative stratigraphy and bedrock surface of the exposed bedrock wall that failed. Seong et al. (2007) suggested that the younger ages of the glacial landforms could also be a consequence of shielding of their surfaces because of a sediment cover. The good preservation of these surfaces indicates that they might have been covered and protected for sometime after the glacier retreated from this area and hence they provide slightly younger ages than the true age for glacier retreat. Thus, although there is a small disparity between glacial landforms and

the rockslide, the strong clustering of ages suggests a Late Glacial age for these landforms. The landslide likely occurred as a result of debuttressing very soon after deglaciation and hence would be paraglacial in origin. The glacial landforms there are probably 12–14 ka as well.

The triggering mechanisms for the extensive Gomboro slope-failure complex are not known. However, it is likely that the structural attitudes of the rocks, weak metasediments, glacially undercut steep slopes of the lower Braldu Valley, and the extensive weathering of the metasediments reducing shear resistance all contributed to the failure. An earthquake might have triggered the initiation of this landslide, however this is not possible to determine.

## 7. Urdokas rockslide complex

The Urdokas ('broken boulders' in the Balti language) rockslide complex (Fig. 1) is one of the major camping sites along Baltoro Glacier on the way to the K2 base camp (Fig. 11). The broken rocks are the result of a major slope failure (Dyhrenfurth, 1939). In fact,



**Fig. 9.** Photograph of part of the irregular lower slip surface of the Gomboro slope-failure complex on the north side of the Braldu River, which is just below the field of view. Note the numerous places where water seeps out below the fragmented rock of the slope failure and the bedrock over which the water flows. The field of view is ~ 150 m.



**Fig. 10.** The central nullah that dissects the shattered and pulverized rock of the Gomboro slope failure. On the lower left occur as many as seven terraces caused by successive rapid wet debris flows that occurred after strong snow melt or rainstorms. Successively slumped terracettes occur in the top center left of the photograph and have risers that ~3 m high.

Urdokas is a rockslide at the sides of Baltoro Glacier where hosts of other slope failures have occurred in the past, but which have now been largely removed by subsequent glacial erosion. Urdokas was preserved because of several fortuitous topographic circumstances. For example, the tributary Yermanendu and Mandu glaciers, rising from the high slopes of Masherbrum (7821 m asl) only some 10 km to the south of Urdokas, have pushed their ice masses directly out into Baltoro Glacier just up-glacier from Urdokas, with the result that the main ice stream is deflected away from the slope failure, thus helping preserve its form. Additionally, Baltoro Glacier also

curves gently north, away from Urdokas, and two bedrock buttresses also occur just upstream and downstream from Urdokas that help deflect the main glacier away from eroding the Urdokas rockslide (Figs. 12 and 13).

The Urdokas rockslide complex comprises granite from the Baltoro plutonic unit, which became detached from the ~6000-m mountain top upslope from it by a small glacier descending obliquely northwest across the upper slopes and eroding away the attachment of the rock to the upper mountain. The result was that a large slab of rock in a mountain peak was then poised some 1–1.5 km above the main Baltoro Glacier valley floor. In addition to its shear resistance being reduced by the transverse glacier erosion above it, an additional causative factor of major importance is a series of low- to moderate-angle plutonic cooling or old sheeting joints that strike nearly east-west and dip north some 25° to nearly 50° in this region. The uppermost transverse glacier erosion had cut down through one of these prominent 40°-dipping joints to detach the rock slab from its uppermost connection, which resulted in the failure of the slope. An isolated small monument of the original bedrock slab still remains on the upper left (west) flank of the failure (Fig. 13).

On the upper right (east) side of the landslide occurs an extensively shattered and well weathered (red staining and lie-sgang rings) leucogranite layer (Fig. 14A) that appears to pass downslope beneath the slope-failure rubble, and perhaps even down beneath what could be a large glide block of otherwise fairly undisturbed bedrock (Fig. 14B and C). The weathering of the shattered leucogranite is probably syn-slope failure, with the shattering being the result of the original landslide, rather than the shattering and weathering occurring either prior to the failure or thereafter.

In plan view the Urdokas rockslide is shaped like a trapezoid, with the longer eastern side (marked U on Fig. 13) representing the greater mass of the slipped and broken slab and the shorter western side having less mass and not projecting itself as far out into Baltoro Glacier valley (Fig. 13). This eastern mass has larger open matrix rock fragments (10–15 m), as well as the probable glide block, whereas the western mass is composed of smaller open-matrix rock blocks (~2–5 m) and a lesser volume. Both lobes have a side-by-side teardrop shape in plan view, with upper slopes of ~30°, with the larger eastern mass also having a lower, more gentle lobe of ~20°, with a ~35° frontal scarp directly above Baltoro Glacier.

The overall Urdokas rockslide is ~0.75 km wide and 1.3 km long from the uppermost contact of the slip surface with the transverse glacier to the toe. The exposed slip surface is ~0.5 km long, and the rockslide mass itself is ~0.8 km long. The thickness of the mass is ~75 m. The H/L ratio of total height (H) to total travel length (L) is ~0.77, which is not large and is reflective of the limited travel distance of the rockslide. This is possibly reflective of combined debuttrressing erosion by Baltoro Glacier, which allowed failure to be initiated in the first place, while coupled with some restricted

**Table 2**  
Sampling locations for boulders, landform, topographic shielding factors,  $^{10}\text{Be}$  concentrations, and  $^{10}\text{Be}$  surface exposure ages for the Gomboro slope-failure complex.

Sample ID	Latitude ( $\pm 0.001\text{N}^\circ$ )	Longitude ( $\pm 0.001\text{E}^\circ$ )	Altitude (m asl)	Shielding factor <sup>a</sup>	$^{10}\text{Be}$ ( $10^4$ atoms/g) <sup>b</sup>	$^{10}\text{Be}$ Exposure age (ka) <sup>c</sup>
K2-36	35.729	75.663	2828	0.94	46.5 $\pm$ 1.25	15.4 $\pm$ 0.4
K2-37	35.729	75.663	2833	0.95	47.6 $\pm$ 1.27	15.6 $\pm$ 0.4
K2-38	35.729	75.663	2832	0.95	48.2 $\pm$ 1.54	15.8 $\pm$ 0.5
K2-39	35.730	75.662	2837	0.95	46.0 $\pm$ 1.25	15.0 $\pm$ 0.4
K2-40	35.730	75.662	2835	0.95	46.1 $\pm$ 1.25	15.0 $\pm$ 0.4
K2-41	35.729	75.663	2839	0.95	40.4 $\pm$ 1.62	13.1 $\pm$ 0.5

Note: Minimum  $^{10}\text{Be}$  ages were calculated using Stone (2000) scaling factors; sea-level high-latitude (SLHL) production rate =  $4.5 \pm 0.3$   $^{10}\text{Be}$  atoms/g quartz per year; zero-erosion rate; and sample thickness of 5 cm; asl—above sea level.

<sup>a</sup> Shielding factor as calculated to correct for topographic barriers using the methods of Nishiizumi et al. (2007).

<sup>b</sup> Atoms of  $^{10}\text{Be}$  per gram of quartz before application of shielding correction factor.

<sup>c</sup> Quoted uncertainty only includes the analytical error.



**Fig. 11.** The Urdokas camp site with its many huge rockslide boulders and open matrix typical of such slope failures.

buttressing by the ice that allowed only limited overall slip. Given the large volume of rock displaced ( $\sim 45 \times 10^6 \text{ m}^3$ ), and the steep slip plane of  $\sim 40^\circ$ , the low H/L displacement ratio argues for glacier buttressing that held the mass partially in place. Even so, the observed recent downwasting of Baltoro Glacier and its nearby tributaries has now additionally debutressed the Urdokas rock-slide, with the result that the open matrix, clast-supported mass is partially reactivated, with plentiful 0.25–1 m wide open ground cracks around many boulders in the upper part of the slope failure.

There are no TCN ages for the Urdokas failure. The freshness of the landform suggest that it formed very recently, probably even late Little Ice Age (LIA), and perhaps only a few hundred years old, as Baltoro Glacier downwasted sufficiently from a LIA of Late Holocene position to allow failure. Sometime after the Early and Middle Holocene during downwasting of Baltoro Glacier, the debutressing of the strongly fractured granites – that dipped on well-developed joint surfaces sloping toward the downwasting ice – caused the granite to slip downward and break into blocks ranging from a few meters in diameter to some that were perhaps 10–15 m across. The leading edge or northernmost toe of the failure may be a large glide block several hundred meters long. If Baltoro Glacier continues to downwaste in future years, Urdokas may become increasingly unstable.

## 8. Discussion

The relations between tectonics, climate, denudation and landscape evolution is clearly complex, as multi-scale surface process domains and feedback mechanisms regulate topographic evolution. Study of the large-scale mass-movement complexes in the Central Karakoram shows that all involved displacement/collapse of large areas at high altitude (i.e., mountain peaks and ridges). Such large-scale mass movements and the numerous rock falls and debris flows within the region supports the view that mass movement is an important denudational agent and does have a significant impact on altering topographic complexity and ultimately influencing the exhumation of bedrock at a variety of scales in the Central Karakoram. Evidence of this includes gneiss dome spatial distribution patterns and uplift variation across the region, as governed by river incision and mass movement (Seong et al., 2008, 2009).

The exhumation of rock from deep within Earth, that is, the movement up into the surficial geomorphology, is collectively achieved by fluvial and glacial erosion, and coupling with mass movement, extensional fault thinning of the surface, or perhaps by buoyant upwelling (Whittington, 2004). The terminology of exhumation can be confusing (England and Molnar, 1990),

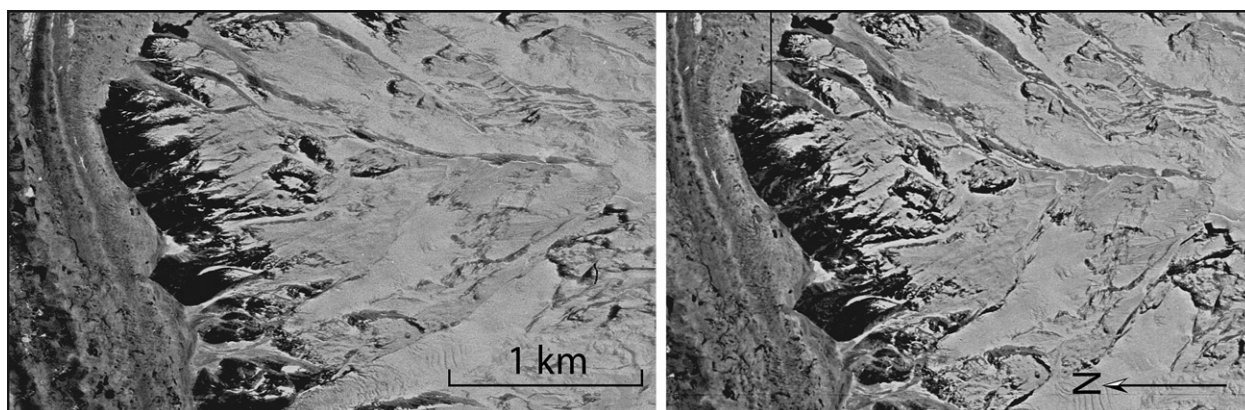


**Fig. 12.** Stereo-pair of declassified Keyhole (KH-11) satellite images of Urdokas area. North is to the left. These images were utilized to make the geomorphology map of Fig. 13, in which north is vertical.

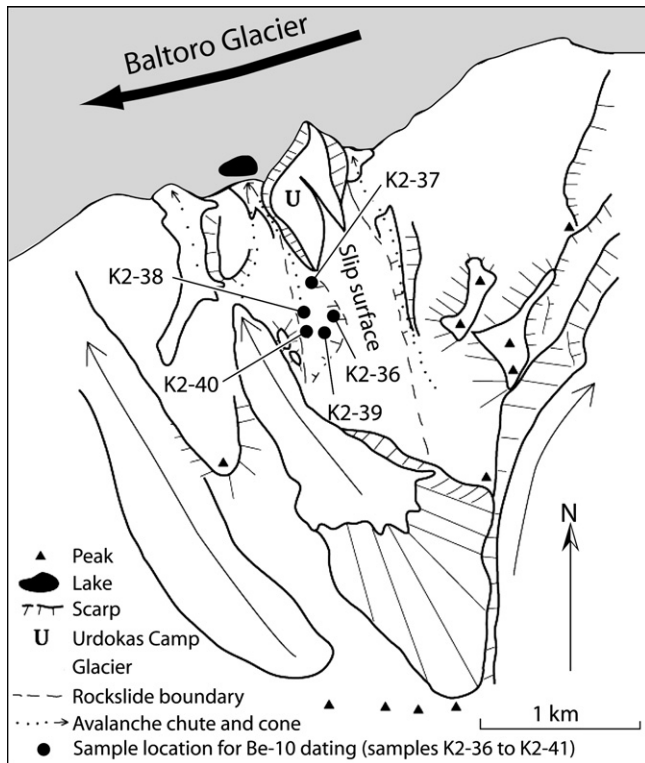


Fig. 13. Geomorphologic map of Urdokas rockslide derived from field assessment and mapping with the Keyhole stereo satellite imagery of Fig. 12.

especially when it is realized that ‘true’ exhumation in the original geomorphic sense (Thornbury, 1954) was used for surficial landforms that were buried first and then subsequently exhumed. However, modern understandings of exhumation have tended to stress extensional collapse of orogens, and denudational unloading caused by numerous geomorphic processes has not been emphasized as much. In contrast, where exhumation has clearly been extremely rapid, yet structural and petrologic evidence for extensional faulting was lacking, ideas and evidence of vigorous surficial erosion have been favored (Shroder and Bishop, 2000; Zeitler et al., 2001a, 2001b; Finnegan et al., 2008), including mass-movement sacking failure (Reinhardt et al., 2007). The relative roles of different surficial processes in denudation and the exhumation of rock in the Central Karakoram have yet to be quantified. New forms of digital terrain analysis may permit a first-order characterization of process domains and active mass movements, although the issues of terrain morphology similarities resulting from multiple processes, and high-magnitude erosion place limits on quantifying spatial and temporal process dominance. Given the shear scale and abundance of landslides and associated landforms in this region, it is reasonable to assume that mass movement is extremely important.

Increasingly in recent years, the role of exhumation of deep crustal rocks has also involved development of better understandings of the origin and development of migmatitic gneiss domes (metamorphic core complexes) (Whitney et al., 2004a; Yin, 2004). The origin of gneiss domes has been much debated, but most commonly they have been viewed as either contractional or extensional (Whitney et al., 2004b). These typically have bounding faults that accommodate differential exhumation relative to the surrounding host rocks (Whittington, 2004). Structural analysis shows that the ductile deformation of the region is partitioned between folding and associated uplift of the Neogene age gneiss



Fig. 14. Views of the Urdokas rockslide. (A) Photograph of the Urdokas slip surface with Urdokas rockslide to the right (north). The lighter toned rock regions in the figure center surrounded by vegetation are the highly fractured leugranite of part of the slip plane (also shown in part B). The upstanding peaks to the upper right are a model of what is thought to have been an approximation of the original situation at Urdokas prior to failure. The smooth slip plane is part of the regional north-dipping joint system in the Baltoro Granite that can also be seen below the snow-covered surface to the upper right. (B) Highly fractured granite just below the Urdokas slip surface. The slip surface is the horizon of this picture. (C) The main Urdokas slope-failure mass from the northeast side. The main boulders of the camp site are out of sight over the top of this ridge. Much of the slope failure in this view may be largely a glide block of granite beneath the grassy slope and exposed as rock to the center left. The foreground is the Baltoro Glacier.

dome area in the southern part of the Karakoram (Skardu Basin to K2) and the Baltoro batholith, and dextral strike-slip motion along the Karakoram Fault (Mahéo et al., 2004). The strong uplift controlled by strain partitioning in an oblique convergent setting, coupled with the lack of lateral expulsion and high erosion rates

helps explain why high temperature mid-crustal rocks occur in the gneiss domes of the huge peaks. Diapiric ascent of molten mid-crustal rocks was forced by the compressive regime, and the zones of rapid uplift were judged to be associated with vigorous erosion due to the likely high incision rates of the large Shyok, Shigar, and Braldu rivers (Seong et al., 2008), as well as the large Biafo–Hispar and Godwin Austen–Baltoro glaciers (Mahéo et al., 2004).

Assessment of the role and magnitude of mass movement in landscape evolution requires more quantitative characterization of the topography, detailed process and landform mapping, and dating of many different types, to obtain a better understanding of the spatial and temporal complexity of mass movement phenomena. Whittington (2004), for example, noted that exhumation rates generally vary from place to place within a terrain, and that erosion by glacial and fluvial processes removes most material from valley floors, which in turn increases the local relief to help achieve an average regional unroofing effect. Whittington (2004) suggested this effect was not characteristic of the local rate of exhumation in any particular place within that terrain, and thus argued that exhumation across normal shear zones would thereby result in significant exhumation of the footwall block but little or none of the hanging wall. Whittington's (2004) views, however, entirely neglected evidence of scale-dependent gravitational mass movement (Shroder and Bishop, 1998), wherein the tops of mountains slide off or subside in massive failures, in which case there is localized high-altitude erosion that is higher in magnitude compared to the valley directly below it. Such high-magnitude slope-failures demonstrate that erosion is not always focused in valley bottoms. Clearly, the spatial and temporal variability of mass movements, and especially massive failures, need to be quantitatively characterized and mapped to better examine the relationships between surface processes, uplift, and landscape evolution.

The 3–4 km of relief, coupled with steep slopes, and high-to-intermediate magnitude and frequency, snow and rainstorms in the Central Karakoram results in considerable potential, gravitational, thermal, and kinetic energy sources that drive the varied surficial erosion processes unroofing the orogen. These processes as noted are chiefly mass movement, glaciers, rivers, and catastrophic floods (Shroder and Bishop, 2000; Seong et al., 2009). The denudation cascade in the Karakoram begins with weathering and mass-movement processes, such as snow and ice avalanches, slow sackungen, rock falls and rockslides, rapid wet debris flows, and profuse talus and colluvial accumulations (Brunsdon et al., 1984; Hewitt, 1988, 1998; Shroder, 1989, 1993; Fort, 1995; Shroder and Bishop, 1998). The products of such mass movement are ubiquitous, piling up to considerable depths on valley floors and sidewalls, or forming the extensive supraglacial debris covers so characteristic of the glaciers of the region.

Strong feedbacks exist between cycles of deep glacial erosion that expose and weaken rocks, as well as deepen valleys, and intensify mass movement processes. Mass movement complexes may involve massive slope failure of whole peaks, which are thought to provide initial mass-movement mobilization of material that subsequent fluvial processes, catastrophic flooding, and later glaciations can progressively remove entirely from the mountain orogen. The four large-scale major mass movement complexes described in this study represent high-magnitude and low- to-moderate frequency events that are exemplary of high-altitude denudation, which were probably triggered during deglaciation. Consequently, these mass movements are most likely the result of climate forcing; as glaciers oscillate and associated streams changes lead to erode the topography, change the relief structure and topographic stress fields, and thereby directly regulating valley-wall slope failure potential and extent. In a study of the nature and timing of large landslides in the Himalaya, Dortch et al. (2009)

showed that 14 out of the 16 dated landslides in the Himalaya occurred during periods of intensified monsoons during the Late Quaternary. Although seismic shaking could not be ruled out as a mechanism for landslide initiation, Dortch et al. (2009) argued for a strong climatic control on landslides. This supports the view that climate, albeit indirectly by paraglacial processes in this study, is an important factor in forcing mass movement that consequently leads to large-scale denudation and landscape evolution. Many of the large landslides throughout this region form in and along mountain crests. During earthquakes seismic shaking is often more intense along mountain ridges and crests. This suggests that earthquakes might have helped initiated many of the landslides in this region. Nevertheless, the evolution of the slopes that fail catastrophically in this region are driven by climate changes that dominantly control the glacial and fluvial erosional systems.

The glacier-massive-failure coupled system removes significant mass at high-altitude, and this likely contributes to the unroofing and exposure of the gneiss domes and Karakoram batholiths. Similar events probably occurred throughout the Quaternary, mainly during times of deglaciation. This suggests that in this region, and similar mountain areas, whenever major glaciations and deglaciation occurs there is also a strong coupling to concomitant major mass movement that allows more spatially extensive denudation.

## 9. Conclusion

This study of the Shigar, Braldu, and Baltoro valleys in the K2 region of the Central Karakoram in Pakistan to ascertain the role of massive slope failures in mountain landscape evolution showed that major mass-movement complexes are prevalent throughout the region. The four major mass-movement complexes include the Ghorohoh rock avalanche, Busper sackung and slope failure, Gomboro slope failure and Urdokas rockslide. TCN dating on two of these landslide complexes show that they occurred in the late Pleistocene and Holocene and were likely related to landscape readjustment during deglaciation. There is empirical evidence that climate forcing governs the magnitude and extent of these failures, and their location is spatially coincident with rapid uplift areas and the exhumation of deeply buried gneiss domes. Such high-altitude focused erosion can exceed valley erosion and contribute significantly to denudational unloading, and perhaps trigger localized exhumation of rock mass. It is also important to note that such localized interrelationships may be highly dependent upon structure to facilitate rapid exhumation.

## Acknowledgments

We should like to thank two anonymous reviewers who provided extremely useful and constructive comments on this paper. This work was funded by National Science Foundation Grant BCS-0242339, National Geographic Society and Natural Sciences and Engineering Research Council of Canada. It was also an outgrowth of NASA- and USGS-funded research for the GLIMS (Global Land Ice Measurements from Space) Regional Center for Southwest Asia at the University of Nebraska at Omaha (NASA OES-02 program, Award NNG04GL84G). Part of this work was undertaken at the Lawrence Livermore National Laboratory under DOE Contract W-7405-ENG-48. The late Syed Hamidullah gave his familiar unstinting advice and most friendly support, as well as providing two hardworking graduate students, Shah Faisal Khan and Mohammed Shahid. Special thanks to the medics of University of Nebraska at Omaha lead by Keith Brown and Bruce Hagen for their support in the field. The University of Nebraska Medical Center provided some 20 medical students and interns under the

direction of Keith Brown and Bruce Hagen who kept us functioning under arduous conditions. Nabir Sabir Expeditions was responsible for logistics under the direction of Rahmat Ali from Hunza and Hajaz from Shigar who guided well and handled some 450 porters, as well as feeding us superbly.

## References

- Balco, G., Stone, J.O., Lifton, N.A., Dunai, T.J., 2008. A simple, internally consistent, and easily accessible means of calculating surface exposure ages or erosion rates from  $^{10}\text{Be}$  and  $^{26}\text{Al}$  measurements. *Quaternary Geochronology* 8, 174–195.
- Beaumont, C., Jamieson, R.A., Nguyen, M.H., Lee, B., 2001. Himalayan tectonics explained by extrusion of a low-viscosity crustal channel coupled to focused surface denudation. *Nature* 414, 738–742.
- Brunsdon, D., Jone, D.K.C., Goudie, A.S., 1984. Particle Size Distribution on Debris Slopes of the Hunza Valley. In: Miller, K. (Ed.), *International Karakoram Project*. Cambridge University Press, Cambridge, pp. 536–579.
- Burbank, D.W., Leland, J., Fielding, E., Anderson, R.S., Brozovic, N., Reed, M.R., Duncan, C., 1996. Bedrock incision, rock uplift and threshold hillslopes in the northwestern Himalayas. *Nature* 379, 505–510.
- Chevalier, M.-L., Ryerson, F.J., Tapponnier, P., Finkel, R.C., Van Der Woerd, J., Li, H., Liu, Q., 2005. Slip-rate measurements on the Karakoram Fault may imply secular variations in fault motion. *Science* 307, 411–414.
- Dainelli, G., 1922. Studi sul glaciale Spedizione Italiana de Filippi nell' Himalaia, Caracorum Turchestan/Cinese (1913–1914). Ser II, 3, p. 658 (in Italian).
- Dortch, J., Owen, L.A., Haneberg, W.C., Caffee, M.W., Dietsch, C., Kamp, U., 2009. Nature and timing of mega-landslides in northern India. *Quaternary Science Reviews* 28, 1037–1056.
- Dyhrenfurth, G.O., 1939. Baltoro. Benno Schwabe & Co, Basel, Switzerland, 194 pp.
- England, P., Molnar, P., 1990. Surface uplift, uplift of rocks, and exhumation of rocks. *Geology* 18, 1173–1177.
- Finnegan, N.J., Hallet, B., Montgomery, D.R., Zeitler, P.K., Stone, J.O., Anders, A.M., Liu, Y., 2008. Coupling of rock uplift and river incision in the Namche Barwa–Gyala Peri massif, Tibet. *Geological Society of America Bulletin* 120, 142–155.
- Fort, M., 1995. The Himalayan glaciation: myth and reality. *Journal of Nepal Geological Society* 11, 257–272.
- Foster, D.A., Gleadow, A.J.W., Mortimer, G., 1994. Rapid Pliocene exhumation in the Karakoram (Pakistan), revealed by fission-track thermochronology of the K2 gneiss. *Geology* 22, 19–22.
- Heim, A., 1932. Bergsturz und Menschenleben. Fretz and Wasmuth, Zurich, 218 pp (in German).
- Hewitt, K., 1988. Catastrophic landslide deposits in the Karakoram Himalaya. *Science* 242, 64–77.
- Hewitt, K., 1989. The altitudinal organisation of Karakoram geomorphic processes and depositional environments. *Zeitschrift für Geomorphologie, N.F. Suppl.-Bd* 76, 9–32.
- Hewitt, K., 1998. Catastrophic landslides and their effects on the Upper Indus streams, Karakoram Himalaya, northern Pakistan. *Geomorphology* 26, 47–80.
- Hewitt, K., 1999. Quaternary moraines vs. catastrophic avalanches in the Karakoram Himalaya, northern Pakistan. *Quaternary Research* 51, 220–237.
- Hewitt, K., 2002. Styles of rock-avalanche depositional complexes conditioned by very rugged terrain, Karakoram Himalaya, Pakistan. In: Evans, S.G., DeGraff, J.V. (Eds.), *Catastrophic Landslides: Effects, Occurrence, and Mechanisms*. Geological Society of America Reviews in Engineering Geology, 15, pp. 345–377.
- Hodges, K.V., 2000. Tectonics of the Himalaya and southern Tibet from two perspectives. *Geological Society America Bulletin* 112, 324–350.
- Hodges, K., August 2006. Climate and the evolution of mountains. *Scientific American*, 72–79.
- Hodges, K.V., Hurtado, J.M., Whipple, K.X., 2001. Southward extrusion of Tibetan crust and its effect on Himalayan tectonics. *Tectonics* 20, 700–809.
- Hodges, K.V., Wobus, C., Ruhl, K., Schildgen, T., Whipple, K., 2004. Quaternary deformation, river steepening, and heavy precipitation at the front of the Higher Himalayan ranges. *Earth and Planetary Science Letters* 220, 379–389.
- Kohl, C.P., Nishiizumi, K., 1992. Chemical isolation of quartz for measurement of in-situ produced cosmogenic nuclides. *Geochimica et Cosmochimica Acta* 56, 3583–3587.
- Koons, P.O., Zeitler, P.K., Chamberlain, C.P., Craw, D., Melzer, A.S., 2002. Mechanical links between river erosion and metamorphism in Nanga Parbat, Pakistan Himalaya. *American Journal of Science* 302, 749–773.
- Koppes, M.N., Montgomery, D.R., 2009. The relative efficacy of fluvial and glacial erosion over modern to orogenic timescales. *Nature Geoscience* 2, 644–647.
- Lal, D., 1991. Cosmic ray labeling of erosion surfaces: in situ nuclide production rates and erosion models. *Earth and Planetary Science Letters* 104, 429–439.
- Mahéo, G., Pecher, A., Guillot, S., Rolland, Y., Delacourt, C., 2004. Exhumation of Neogene gneiss domes between oblique crustal boundaries in south Karakoram (northwest Himalaya, Pakistan). In: Whitney, D.L., Teyssier, C., Siddoway, C.S. (Eds.), *Gneiss Domes in Orogeny*. Geological Society of America Special Paper, 380, pp. 141–154.
- Molnar, P., 1988. A review of the geophysical constraints on the deep structure of the Tibetan Plateau, the Himalaya and the Karakoram, and their tectonic implications. *Philosophical Transactions of the royal Society of London, Series A* 326, 33–88.
- Molnar, P., Tapponnier, P., 1975. Cenozoic tectonics of Asia: effects of a continental collision. *Science* 189, 419–426.
- Nishiizumi, K., Imamura, M., Caffee, M.W., Southon, J.R., Finkel, R.C., McAninch, J., 2007. Absolute calibration of  $^{10}\text{Be}$  AMS standards. *Nuclear Instruments and Methods in Physics Research Section B* 258 (2), 403–413.
- Oestrich, K., 1906. Die Täler des nordwestlichen Himalaya. In: *Ergänzungsheft zu Petermanns Mitteilungen*, vol. 155. Justus Perthes, Gotha (in German).
- Owen, L.A., Caffee, M.W., Finkel, R.C., Seong, B.Y., 2008. Quaternary glaciations of the Himalayan-Tibetan orogen. *Journal of Quaternary Science* 23, 513–532.
- Phillips, F.M., 1995. Cosmogenic chlorine-36 accumulation: a method for dating quaternary landforms. In: Rutter, N.W., Catto, N.R. (Eds.), *Dating Methods for Quaternary Deposits*. Geological Association of Canada, Newfoundland, St. John's, pp. 61–66.
- Phillips, F.M., Zreda, M.G., Flinsch, M.R., Elmore, D., Sharma, P., 1996. A reevaluation of cosmogenic  $^{36}\text{Cl}$  production rates in terrestrial rocks. *Geophysical Research Letters* 23, 949–952.
- Phillips, F.M., Stone, W.D., Fabryka-Martin, J.T., 2001. An improved approach to calculating low-energy cosmic-ray neutron fluxes at the land/atmosphere interface. *Chemical Geology* 17, 689–701.
- Reinhardt, L.J., Dempster, T.J., Shroder Jr., J.F., Persano, C., 2007. Tectonic denudation and topographic development in the Spanish Sierra Nevada. *Tectonics* 26 (3). doi:10.1029/2006TC001954 TC3001.
- Robinson, A.C., 2009. Evidence against Quaternary slip on the northern Karakoram Fault suggests kinematic reorganization at the western end of the Himalayan-Tibetan orogen. *Earth and Planetary Science Letters* 286, 158–170.
- Searle, M.P., 1991. *Geology and Tectonics of the Karakoram Mountains*. John Wiley & Sons, Chichester, 358 pp.
- Searle, M.P., Rex, A.J., Tirrul, R., Rex, D.C., Barnicoat, A., Windley, B.F., 1989. Metamorphic, magmatic, and tectonic evolution of the central Karakoram in the Biafo-Baltoro-Hushe regions of northern Pakistan. In: Malinconico, L.L., Lillie, R. J. (Eds.), *Tectonics of the Western Himalayas*. Geological Society of America Special Paper, 232, pp. 47–73.
- Seong, Y.B., Owen, L.A., Bishop, M.P., Bush, A.B.G., Clendon, P., Copland, L., Finkel, R., Kamp, U., Shroder Jr., J.F., 2007. Quaternary glacial history of the Central Karakoram. *Quaternary Science Reviews* 26, 3384–3405.
- Seong, Y.B., Owen, L.A., Bishop, M.P., Bush, A.B.G., Clendon, P., Copland, L., Finkel, R., Kamp, U., Shroder Jr., J.F., 2008. Rates of fluvial bedrock incision within an actively uplifting orogen: central Karakoram Mountains, northern Pakistan. *Geomorphology* 97, 274–286.
- Seong, Y.B., Bishop, M.P., Bush, A.B.G., Clendon, P., Copland, L., Finkel, R., Kamp, U., Owen, L.A., Shroder Jr., J.F., 2009. Landforms and landscape evolution in the Skardu, Shigar and Braldu valleys, central Karakoram mountains. *Geomorphology* 103, 251–267.
- Shroder Jr., J.F., 1989. Slope failure: extent and economic significance in Afghanistan and Pakistan. In: Brabb, E.E., Harrod, B.L. (Eds.), *Landslides: Extent and Economic Significance in the World*. A.A. Balkema, Rotterdam, Netherlands, pp. 325–341.
- Shroder Jr., J.F., 1993. Himalaya to the sea: geomorphology and the Quaternary of Pakistan in the regional context. In: Shroder Jr., J.F. (Ed.), *Himalaya to the Sea: Geology, Geomorphology, and the Quaternary*. Routledge Press, London, pp. 1–42.
- Shroder Jr., J.F., 1998. Slope failure and denudation in the western Himalaya. *Geomorphology* 26, 81–105.
- Shroder Jr., J.F., Bishop, M.P., 1998. Mass movement in the Himalaya: new insights and research directions. *Geomorphology* 26, 13–35.
- Shroder Jr., J.F., Bishop, M.P., 2000. Unroofing the Nanga Parbat Himalaya. In: Khan, M. A., Treloar, P.J., Searle, M.P., Jan, M.Q. (Eds.), *Tectonics of the Western Himalaya and Karakoram*. Geological Society of London Special Publication, vol. 170, pp. 163–179.
- Stone, J.O., 2000. Air pressure and cosmogenic isotope production. *Journal of Geophysical Research* 105, 23753–23759.
- Stone, J.O., Fifield, L.K., Allan, G.L., Cresswell, R.G., 1996. Cosmogenic chlorine-36 from calcium spallation. *Geochimica et Cosmochimica Acta* 60, 679–692.
- Tapponnier, P., Molnar, P., 1979. Active faulting and Cenozoic tectonics of the Tien Shan, Mongolia and Baykalia regions. *Journal of Geophysical Research* 84, 3425–3459.
- Thornbury, W.D., 1954. *Principles of Geomorphology*. John Wiley & Sons, New York, 618 pp.
- Whitney, D.L., Teyssier, C., Siddoway, C.S. (Eds.), 2004a. *Gneiss Domes in Orogeny*. Geological Society of America Special Paper, vol. 380.
- Whitney, D.L., Teyssier, C., Vanderhaeghe, O., 2004b. Gneiss domes and crustal flow. In: Whitney, D.L., Teyssier, C., Siddoway, C.S. (Eds.), *Gneiss Domes in Orogeny*. Geological Society of America Special Paper, vol. 380, pp. 15–33.
- Whittington, A.G., 2004. The exhumation of gneiss domes in divergent wedges: Geometrical concepts and examples from the Himalayan syntaxes. In: Whitney, D.L., Teyssier, C., Siddoway, C.S. (Eds.), *Gneiss Domes in Orogeny*. Geological Society of America Special Paper, vol. 380, pp. 35–46.
- Wobus, C.W., Hodges, K.V., Whipple, K.X., 2003. Has focused denudation sustained active thrusting at the Himalayan topographic front? *Geology* 31, 861–864.
- Yin, A., 2004. Gneiss domes and gneiss dome systems. In: Whitney, D.L., Teyssier, C., Siddoway, C.S. (Eds.), *Gneiss Domes in Orogeny*. Geological Society of America Special Paper, vol. 380, pp. 1–14.
- Zeitler, P.K., Koons, P.O., Bishop, M.P., Chamberlain, C.P., Craw, D., Edwards, M.A., Hamidullah, S., Jan, M.Q., Khan, M.A., Khattak, M.U.K., Kidd, W.S.F., Mackie, R.L., Meltzer, A.S., Park, S.K., Pecher, A., Poage, M.A., Sarker, G., Schneider, D.A., Seeber, L., Shroder, J.F., 2001a. Crustal reworking at Nanga Parbat, Pakistan: metamorphic consequences of thermal-mechanical coupling facilitated by erosion. *Tectonics* 20, 712–728.
- Zeitler, P.K., Meltzer, A., Koons, P.O., Craw, D., Hallet, B., Chamberlain, C.P., Kidd, W.S.F., Park, S.K., Seeber, L., Bishop, M., Shroder Jr., J.F., 2001b. Erosion, Himalayan geodynamics, and the geomorphology of metamorphism. *GSA Today* 11, 4–9.